

Effects of Ion Orbits Due to Potential Formation on Transverse Ion Transport in the Thermal Barrier Region of GAMMA10

H. SAIMARU, I. KATANUMA, Y. MIZOGUCHI, K. YASHIRO and T. CHO

*Plasma Research Center, University of Tsukuba,
1-1-1 Tennoudai, Tsukuba, Ibaraki 305-8577, Japan*

(Received 4 December 2006 / Accepted 1 March 2007)

Transverse ion loss in the thermal barrier region of the GAMMA10 tandem mirror is investigated with the mapping equations of ion drift orbits. The effects of a non-axisymmetric electrostatic potential in the thermal barrier are taken into account. The local stability of orbits and its diffusion are calculated numerically and these are compared with the results of A.B. Rechester and R.B. White [1]. It is found that there are two kinds of the transverse ion transport. One is chaotic ion orbits due to unstable ion drift, which cause cross-field ion diffusion. Another is the enhanced effects of ion radial step sizes on the transverse diffusion, because banana-like ion drift orbits appear due to the non-axisymmetric electrostatic potential formation.

© 2007 The Japan Society of Plasma Science and Nuclear Fusion Research

Keywords: drift shear, fixed point, diffusion, stable region, tangent mapping

DOI: 10.1585/pfr.2.S1086

1. Introduction

The GAMMA10 tandem mirror has the axisymmetric end-mirror cells, where ion density in the thermal barrier is much less than that in the central cell, which suggests that ions escape rapidly from the thermal barrier region. It is observed that plug potential profile is not axisymmetric [2]. And, the calculation of ion orbits reveals that there is a transition from regular orbits to chaotic ones as the non-axisymmetric electrostatic potential increases [3].

In the recent research by mapping equation, the diffusion of ions do not occur as long as only one mode perturbation is added to the axisymmetric electrostatic potential, but, when one more small amplitude of additional perturbations are added further, the diffusion of ions is observed [4].

In the present work, one mode of perturbation is added to the electrostatic potential corresponding to radial $\mathbf{E} \times \mathbf{B}$ drift shear as the amount of azimuthal shift $\Delta\theta = \psi^{1/2}$, and resultant mapping equation is studied. The details of ion orbits (fixed points, local stability of orbits, diffusion) are analyzed by the mapping equation. The diffusion coefficient is compared with that obtained by A.B. Rechester and R.B. White [1].

2. Mapping Model

Radial and azimuthal intersection points of an ion with an equatorial plane at the midplane in the mirror cell are represented by the mapping equation [4]. Electrostatic potential profile in the plug region is assumed as

$$\begin{aligned} \phi(\psi, \theta, z) &= \phi_0 \left[1 - (\psi/\psi_w)^{3/2} \right] \quad \text{for } z \leq z_p - \delta z_p \\ \phi(\psi, \theta, z) &= \phi_1 \cos \theta \quad \text{for } z > z_p - \delta z_p, \end{aligned} \quad (1)$$

where z_p is the axial coordinate at the plug, and δz_p is the half width of an axial profile of plug potential. Henceforth we adopt the coordinates (ψ, θ, z) , where magnetic field \mathbf{B} is represented by $\mathbf{B} = \nabla\psi \times \nabla\theta$. We use the following mapping equation

$$\begin{aligned} \psi_{n+1} &= \psi_n + K \sin \theta_n \\ \theta_{n+1} &= \theta_n + \psi_{n+1}^{1/2}. \end{aligned} \quad (2)$$

Here K is a function of ϕ_0 and ϕ_1 in Eq. (1). Noting that $\psi = B_z r^2/2$ in the paraxial approximation, the profile of Eq. (1) is $\phi(r, z) \propto [1 - (r/r_w)^3]$. We include the effects of $\mathbf{E} \times \mathbf{B}$ drift shear for $\Delta\theta_n \equiv \theta_{n+1} - \theta_n = \psi_{n+1}^{1/2}$ in Eq. (2). Analytically, some fixed points independent of K is obtained from Eq. (2) as

$$(\psi_{fixed}, \theta_{fixed}) = ((2\pi m)^2, \pi n) \text{ for integers } m, n \quad (3)$$

where the relation

$$\psi_{n+k} = \psi_n, \quad \theta_{n+k} = \theta_n + 2\pi m \quad (4)$$

is satisfied.

The locations of fixed points dependent on K are determined numerically. In Fig. 1, the points at the intersection of each curves are fixed points for $K = 10$, while orbits of 49 ions are plotted by dots for the same amplitude of K , where initial positions of the ions are evenly distributed in the region of $0 \leq \psi \leq 20\pi^2$ and $0 \leq \theta < 2\pi$. The solid curves are given by $\psi_{n+1} = \psi_n$, and the broken curves (1 period) are the lines of $\theta_{n+1} = \theta_n + 2\pi m$, and the dotted curves (2 period) represent the lines of $\theta_{n+1} = \theta_n + (2m + 1)\pi$. The

author's e-mail: Saimaru@prc.tsukuba.ac.jp

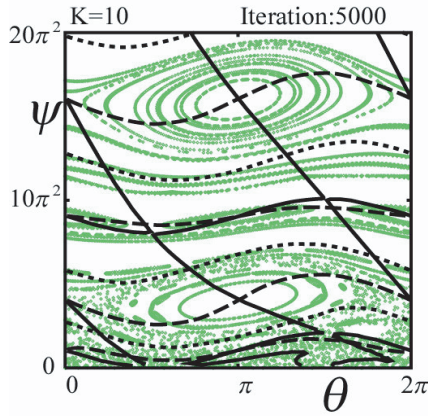


Fig. 1 The dependence of the locations of fixed points on K are evaluated numerically. The points at the intersection of each curves are fixed points for $K = 10$, while orbits of 49 ions are plotted in dots for same K , where initial positions of the ions are evenly distributed in the region of $0 \leq \psi \leq 20\pi^2$ and $0 \leq \theta < 2\pi$.

other fixed points, which depend on K , can be seen in the figure in addition to those given by Eqs. (3) and (4). And, the obtained ion orbits show that the numerical positions of fixed points are valid.

The stability of a fixed point is determined by a tangent mapping as mapping of adjacent points (ψ, θ) and $(\psi + \delta\psi, \theta + \delta\theta)$. After k iterations, Eq. (2) reduced to the tangent mapping

$$\begin{pmatrix} \delta\psi_{n+k} \\ \delta\theta_{n+k} \end{pmatrix} = M \begin{pmatrix} \delta\psi_n \\ \delta\theta_n \end{pmatrix} \quad (5)$$

$$M = \begin{pmatrix} \frac{\partial\psi_{n+k}}{\partial\psi} & \frac{\partial\psi_{n+k}}{\partial\theta} \\ \frac{\partial\theta_{n+k}}{\partial\psi} & \frac{\partial\theta_{n+k}}{\partial\theta} \end{pmatrix} = \prod_{j=1}^{k-1} \begin{pmatrix} 1 & K \cos \theta_{n+j} \\ \frac{1}{2\psi_{n+j+1}} & 1 + \frac{K \cos \theta_{n+j}}{2\psi_{n+j+1}} \end{pmatrix}, \quad (6)$$

where the derivatives are evaluated at the fixed points. The behavior around the fixed points are described by the eigen equation

$$\lambda^2 - \text{Tr}(M)\lambda + \det(M) = 0, \quad (7)$$

Here $\det(M) = 1$ because of area preserving map of Eq. (2), and λ is the eigenvalue of matrix M which gives the local stability of any points. In the case of $\text{Tr}(M)^2 - 4 < 0$, the eigenvalues are complex and so the tangent space orbit is stable. Figure 2 plots the stable (gray) and unstable (white) regions calculated by Eq. (5). Here the same orbits as in Fig. 1 are plotted. As K increases, the unstable region expands, the stable and unstable regions admix each other in the region of small ψ . In Fig. 2, we observe that stochastic orbits are dominate in that region and regular orbits exist in the region $\psi \geq 2\pi^2$.

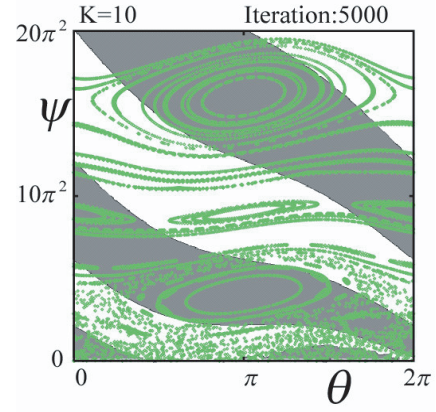


Fig. 2 The stable (gray) and unstable (white) regions are calculated by Eq. (5). The same orbits as in Fig. 1 are plotted.

For the regular orbits, the phase trajectory can be obtained by the use of the secular perturbation theory. Equation (2) can be rewritten as differential equation by introduction of the delta function in the equation of motion:

$$\frac{d\psi}{dt} = \delta(t - n) K \sin \theta \quad (8)$$

and

$$\frac{d\theta}{dt} = \psi^{1/2}, \quad (9)$$

where the time variable t is measured in units of the number of bounces n . Equations (8) and (9) have a Hamiltonian form

$$H = 2\psi^{3/2}/3 + \sum_{m=-\infty}^{\infty} e^{i2\pi mt} K \cos \theta, \quad (10)$$

with ψ and θ as the canonical coordinates, where a fourier representation of the delta function is used. In the region of very small ψ , i.e.,

$$(\theta_{n+1} - \theta_n) \ll 2\pi, \quad (11)$$

Eq. (10) can be averaged over t to obtain a constant of motion;

$$\langle H \rangle = 2\psi^{3/2}/3 + K \cos \theta = C, \quad (12)$$

which gives the trajectories near $\psi = 0$.

Furthermore, transform to a coordinate system $(\hat{\psi}, \hat{\theta})$ around the period 1 fixed point of Eq. (3) is carried out as

$$\hat{\psi} = \psi - \psi_{\text{fixed}}, \quad \hat{\theta} = \theta - \theta_{\text{fixed}}, \quad (13)$$

so that the following relation is satisfied.

$$\hat{\theta}_{n+1} - \hat{\theta}_n \ll 2\pi. \quad (14)$$

Using the variables $(\hat{\psi}, \hat{\theta})$, Eqs. (8) and (9) take the form

$$\frac{d\hat{\psi}}{dt} = \delta(t - n) K \sin \hat{\theta}, \quad (15)$$

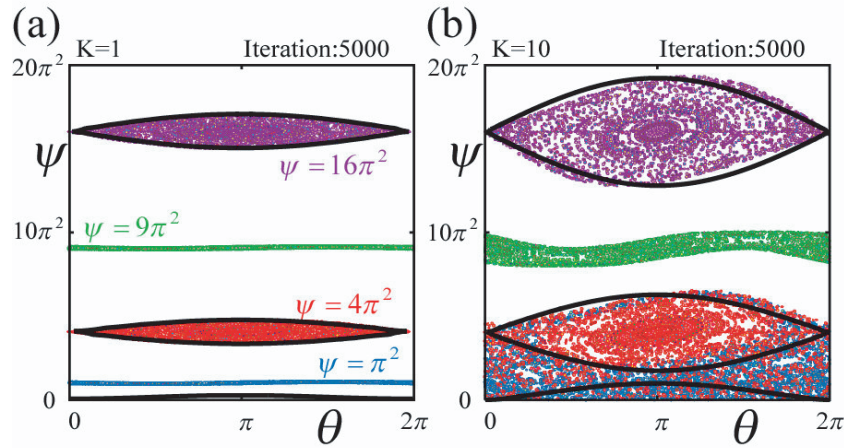


Fig. 3 The separatrix curves for Eqs. (12) and (18) are plotted by bold solid curves respectively for $K = 1, 10$, while the orbits of 3000 ions are plotted in dots, where initial positions of the ions are evenly distributed in the region of $0 \leq \theta < 2\pi$ at the four radial positions $\psi = \pi^2, 4\pi^2, 9\pi^2, 16\pi^2$.

$$\frac{d\hat{\theta}}{dt} = \frac{\hat{\psi}}{2\psi_{fixed}^{1/2}}. \quad (16)$$

Equations (14) and (15) can be integrated to obtain a new Hamiltonian

$$\hat{H} = \frac{\hat{\psi}^2}{4\psi_{fixed}^{1/2}} + \sum_{m=-\infty}^{\infty} e^{i2\pi mt} K \cos \hat{\theta}. \quad (17)$$

If the motion in the $\hat{\psi} - \hat{\theta}$ phase plane is slow on the time scale t , Eq. (17) can be averaged over t to give the averaged new Hamiltonian

$$\langle \hat{H} \rangle = \frac{\hat{\psi}^2}{4\psi_{fixed}^{1/2}} + K \cos \hat{\theta} = C, \quad (18)$$

which describes the trajectories near the period 1 fixed points. The equi-contour surfaces of $\langle H \rangle$ and $\langle \hat{H} \rangle$ consist of closed orbits encircling a fixed point, where a separatrix is given by the maximum value of C when $C = K$. In Fig. 3, the separatrix curves for Eqs. (12) and (18) are plotted by bold solid curves respectively for $K = 1, 10$, while the orbits of 3000 ions are plotted in dots, where initial positions of the ions are evenly distributed in the region of $0 \leq \theta < 2\pi$ at the four radial positions $\psi = \pi^2, 4\pi^2, 9\pi^2, 16\pi^2$. For $K = 1$, the separatrix curves around period 1 fixed points are obtained in Fig. 3 (a), and for $K = 10$ the separatrix curves are different from the boundary of ion motions, in the region of lower ψ in Fig. 3 (b).

3. Numerical Results for Diffusion Coefficients

We now turn to diffusion for ions. A diffusion coefficient is given by

$$D_n = \frac{\langle \Delta\psi_n^2 \rangle}{2n} = \frac{1}{2n} \sum_{j=1}^N \frac{(\psi_n(j) - \psi_0(j))^2}{N}, \quad (19)$$

where n is iteration number and N is total test ion number, and the average is taken over test ions. The quasilinear diffusion coefficient for mapping of Eq. (2) is written as

$$D_{QL} = \frac{D_1}{2} = \frac{1}{4\pi} \int_0^{2\pi} (\Delta\psi)^2 d\theta = \frac{K^2}{4}, \quad (20)$$

on the assumption that $K \gg 1$. The diffusion coefficient in Eq. (19) approaches that in Eq. (20) [5]. For the standard mapping, where

$$\begin{aligned} \psi_{n+1} &= \psi_n + K \sin \theta_n \\ \theta_{n+1} &= \theta_n + \psi_{n+1}, \quad \text{mod } 2\pi, \end{aligned} \quad (21)$$

the analytical diffusion coefficient for large K was obtained by Rechester and White [1] as

$$D_n = \frac{K^2}{2} \left[\frac{1}{2} - J_2(K) - J_1^2(K) + J_2^2(K) + J_3^2(K) \right]. \quad (22)$$

Figure 4 shows the numerical results of diffusions by calculating Eq. (2), and Eq. (21) where the periodic boundary condition of $\text{mod } 2\pi$ for ψ is removed, and diffusion by calculating the following mapping equation

$$\begin{aligned} \psi_{n+1} &= \psi_n + K \sin \theta_n \\ \theta_{n+1} &= \theta_n + \psi_{n+1}^2, \end{aligned} \quad (23)$$

i.e., $\Delta\theta_n = \psi_{n+1}^2$. The diffusion coefficients D_{50} for 3000 ions are calculated excluding the orbits trapped around the fixed points, where initial positions of the ions are evenly distributed in the region of $0 \leq \theta < 2\pi$ at $\psi = \pi^2$ in Fig. 4 (a) and $\psi = 17\pi^2$ in Fig. 4 (b). The dots give the numerical results of D_{50} normalized to quasilinear value in

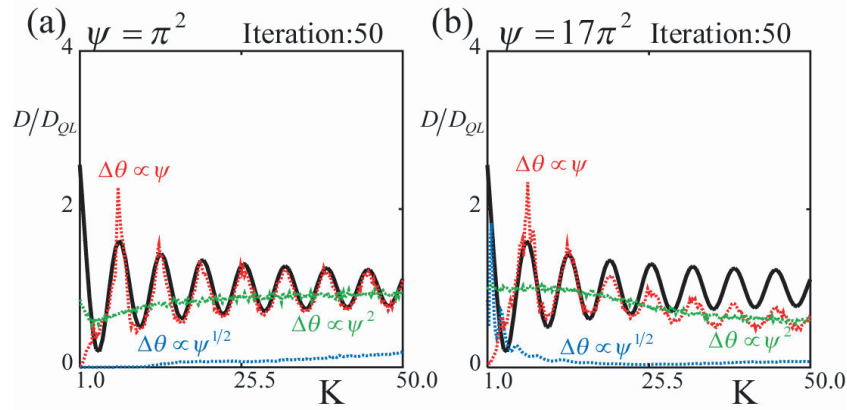


Fig. 4 The dots give the numerical results of D_{50} normalized to quasilinear value in Eq. (20), where the amplitude of perturbation K is varied. The bold solid curve shows the analytical result of Eq. (22).

Eq. (20), where the amplitude of perturbation K is varied. The bold solid curve shows the analytical result of Eq. (22). The result for mapping Eq. (2) in Fig. 4(b) suggests that the existence of non-diffusing orbits lying inside the regular orbits enlarges the diffusion coefficient, because regular motions are dominant over the chaotic motions in the region of large ψ for this mapping.

4. Summary

The mapping equation in non-axisymmetric potential having radial $\mathbf{E} \times \mathbf{B}$ drift shear of electric field is given in this study, in the case of azimuthal shift $\Delta\theta = \psi^{1/2}$. By the numerical calculation of this mapping equation, the positions of period 1 fixed points and the stability of ion orbits around the fixed points are analyzed. The new Hamiltonian obtained by secular perturbation theory gives the separatrix curves around elliptic fixed points applicable for small amplitude K . The diffusion coefficients for mapping equations having several $\mathbf{E} \times \mathbf{B}$ drift shears are estimated and

compared with the analytical result obtained by Rechester and White, in order to examine the effects of non-diffusing orbits lying inside regular orbits on the diffusion coefficient. The numerical result by the mapping Eq. (2) having the drift shear $\Delta\theta = \psi^{1/2}$ shows that the orbits lying inside regular orbits contributes to the growth of diffusion coefficient in the region of large ψ .

- [1] A.B. Rechester and R.B. White, Phys. Rev. Lett. **44**, 1586 (1980).
- [2] K. Yatsu, T. Cho, M. Hirata, H. Hojo, M. Ichimura, K. Ishii *et al.*, Nucl. Fusion **41**, 613 (2001).
- [3] I. Katanuma, H. Saimaru, Y. Tatematsu, T. Saito, K. Ishii, T. Cho *et al.*, J. Plasma Fusion Res. SERIES **6**, 461 (2004).
- [4] H. Saimaru, I. Katanuma, Y. Sasagawa, T. Cho, Fusion Engineering and Design **81**, 2801 (2006).
- [5] A.J. Lichtenberg and M.A. Lieberman, *Regular and Chaotic Dynamics* (Springer-Verlag, Inc., New York, 1992) p.334.